sensors

MDPI

Communication

Piezoresistance Characterization of Silicon Nanowires in Uniaxial and Isostatic Pressure Variation

Elham Fakhri [1,*], Rodica Plugaru [2], Muhammad Taha Sultan [1,3], Thorsteinn Hanning Kristinsson [1], Hákon Örn Árnason [1], Neculai Plugaru [2], Andrei Manolescu [1], Snorri Ingvarsson [3] and Halldor Gudfinnur Svavarsson [1,*]

[1] Department of Engineering, Reykjavik University, Menntavegur 1, 102 Reykjavik, Iceland
[2] National Institute for Research and Development in Microtechnologies-IMT Bucharest, 077190 Voluntari, Romania
[3] Science Institute, University of Iceland, Dunhaga 3, 107 Reykjavik, Iceland
* Correspondence: elhamf20@ru.is (E.F.); halldorsv@ru.is (H.G.S.)

Abstract: Silicon nanowires (SiNWs) are known to exhibit a large piezoresistance (PZR) effect, making them suitable for various sensing applications. Here, we report the results of a PZR investigation on randomly distributed and interconnected vertical silicon nanowire arrays as a pressure sensor. The samples were produced from p-type (100) Si wafers using a silver catalyzed top-down etching process. The piezoresistance response of these SiNW arrays was analyzed by measuring their I-V characteristics under applied uniaxial as well as isostatic pressure. The interconnected SiNWs exhibit increased mechanical stability in comparison with separated or periodic nanowires. The repeatability of the fabrication process and statistical distribution of measurements were also tested on several samples from different batches. A sensing resolution down to roughly 1 mbar pressure was observed with uniaxial force application, and more than two orders of magnitude resistance variation were determined for isostatic pressure below atmospheric pressure.

Keywords: silicon nanowires; MACE; piezoresistivity

Citation: Fakhri, E.; Plugaru, R.; Sultan, M.T.; Hanning Kristinsson, T.; Örn Árnason, H.; Plugaru, N.; Manolescu, A.; Ingvarsson, S.; Svavarsson, H.G. Piezoresistance Characterization of Silicon Nanowires in Uniaxial and Isostatic Pressure Variation. *Sensors* **2022**, *22*, 6340. https://doi.org/10.3390/s22176340

Academic Editor: Haim Abramovich

Received: 25 July 2022
Accepted: 18 August 2022
Published: 23 August 2022

Publisher's Note: MDPI stays neutral with regard to jurisdictional claims in published maps and institutional affiliations.

Copyright: © 2022 by the authors. Licensee MDPI, Basel, Switzerland. This article is an open access article distributed under the terms and conditions of the Creative Commons Attribution (CC BY) license (https://creativecommons.org/licenses/by/4.0/).

1. Introduction

Low-dimensional structures may possess unique mechanical, electrical, optical, and thermoelectric properties. Particularly, silicon nanowires (SiNWs) have demonstrated properties suitable for various advanced applications [1–3], including low-cost thermoelectric devices and chemo-biological sensors with ultrahigh sensitivity [4,5]. The integration of SiNWs in electronic devices is favoured by their compatibility with the well-established Si-SiO_2 electronic industrial technology. Bulk silicon has been known for a while to exhibit high piezo resistance (PZR) effect [6]. In bulk semiconductors, the PZR-effect takes place, in principle, due to a change in the electronic structure and modification of the charge-carriers effective masses. This phenomenon has found practical applications in many Si-based devices, such as pressure transducers [7], cantilevers for atomic force microscopy [8], accelerometers [9], biosensors [10], and multi-axis force sensing tools [11].

Recently, nanowires have been shown to possess the ability to significantly increase the PZR response [12]. A giant PZR was observed in p-doped SiNWs with diameters of 50 nm to 350 nm and a length of microns initially under tensile uniaxial stress [13]. However, the PZR effect in n-doped nanowires was found to be comparable to that in the bulk counterpart, both for tensile and compressive uniaxial stress [14].

On the theoretical side, the origin of the PZR effect in SiNWs has long been under debate, and most frequently, it is referred to as anomalous PZR [15]. It has been related to quantum confinement effects [16], surface charge effects [17–19], strain-induced bandgap shift [20], or changes in the charge carrier's effective masses [21]. A complex model

incorporating these mechanisms has been proposed in order to analytically quantify the PZR effect in silicon [22].

A survey of several PZR sensors based on SiNWs, e.g., cantilever [23], opto-mechanical sensor [24], flexible pressure sensor [18], or breath detector [19], shows that different methods have been used for fabricating the SiNWs, such as vapor-liquid-solid (VLS), laser ablation, and metal-assisted catalyzed etching (MACE) [25]. Among these methods, MACE is the simplest and most versatile one [26]. It relies on catalyzed etching with assistance from a perforated metal template film (typically gold or silver) [27] or randomly distributed metallic nanoparticles (typically gold or silver) [28,29] spread on the Si-wafer. To date, studies have been focused on using different gas types to apply direct pressure on SiNWs, either single SiNW or arrays of SiNWs [19,30], and have neglected the SiNWs response under isostatic pressure, which creates a load uniformly distributed on the sample surface. Here, we report on the PZR effect in SiNWs obtained by MACE under uniaxial compression load as well as isostatic pressure in a vacuum chamber. We find that the interconnected SiNWs are mechanically stronger and functionally more stable compared with the arrays of separated wires under applied uniaxial pressure. They show higher PZR sensitivity under isostatic pressure variation. We also demonstrate a simple, low-cost, and reproducible fabrication method for a robust and sensitive pressure sensor.

2. Materials and Methods

2.1. Fabrication of SiNWs

Arrays of interconnected SiNWs were fabricated by silver (Ag) MACE in a three-step process, from p-type, single-side polished 525 μm-thick Si wafers, with resistivity, ρ, of 10 Ω cm to 20 Ω cm. The nanowire patterns were made on areas of about 1 cm^2 on the polished side of the wafers. The sequence of steps used to prepare the SiNW areas is as follows:

1. Deposition of metal catalyst: Ag nanoparticles were deposited on the surface of the Si wafers by immersing the wafers in a solution of 3 M HF and 1.5 M $AgNO_3$ for 60 s.
2. Wire etching: The samples were etched by immersing them in HF:H_2O_2 (5M:0.4M) solution to obtain vertically aligned SiNWs.
3. Removal of residual Ag nanoparticles: Samples were immersed in 20% *w/v* HNO_3 to remove residual silver particles. A more detailed description can be found in Refs. [28,29].

Subsequently, 150 nm-thick aluminum electrodes were deposited on the samples by electron beam evaporation (Polyteknik Cryofox Explorer 600 LT). For the uniaxial measurements, the electrodes were deposited on the top and backside of the samples, while for the isostatic pressure measurements, the electrodes were made co-planar.

Four sets of interconnected SiNWs samples, denoted as follows, were prepared by varying the etching time: A (1 min), B (3 min), C (5 min), and D (7 min) were made for uniaxial pressure application, and sample E (40 min) was made for isostatic pressure testing.

Additionally, periodic SiNWs, such as sample F, were made as described in the Supplementary Material. Table 1 shows the list of the samples with corresponding etching times and length.

A scanning electron microscope (SEM, Zeiss Supra 35) was used to characterize the SiNW's geometry. Top and cross-sectional SEM images were used to estimate the average diameter of the wires. The Gwyddion software for data visualization and analysis was applied to surface SEM images in order to estimate the total top area of the wires. Figure 1 shows (a,b) the cross-section of the wire array and (c) the surface area of SiNWs obtained after 7 min etching. It is worth mentioning here that the SEM analysis was carried out on the sample prior to the removal of Ag nanoparticles, which are visualized as bright spots at the base of the nanowires in the cross-section.

Table 1. List of samples with different etching times and corresponding lengths. Samples A, B, C, D, and E are random wires, and sample F is with periodic wires (shown in the Supplementary Material).

Sample	Etching Time (min)	SiNW Length (µm)
A	1	0.7
B	3	1.5
C	5	2.2
D	7	3
E	40	10
F	5	0.65

As can be seen in the top-view image, the wires are partly interconnected, forming a continuous rigid structure. Further, also seen from place to place are free-standing nanowires forming bundles. Such bundle formation may take place because of capillary forces acting during the drying process following the wet-etching step. In the cross-sectional image, one may observe that the length of the wires is relatively homogeneous, around 3 µm, and their typical diameter is approximately 150 nm. According to Peng et al. [5], porosity plays an essential role in the PZR response, which increases with increased porosity. The porosity is most conveniently controlled by the concentration of Ag deposition solution and etching time. In a previous study [28], it was demonstrated that the SiNWs porosity was highly affected by the concentration of the $AgNO_3$ during the Ag deposition. A 1.5 mM $AgNO_3$ (as used for samples A–D) provided highly porous SiNWs with maximum photoluminescence spectra intensity.

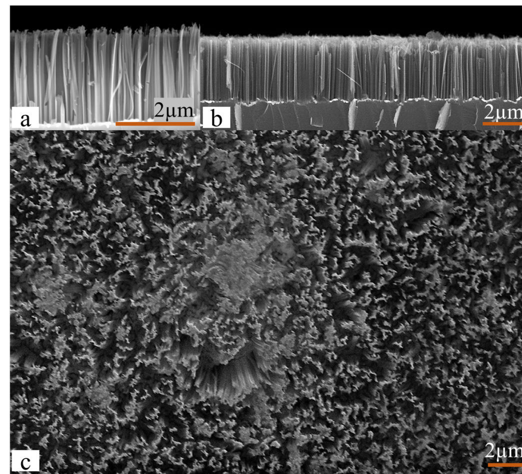

Figure 1. SEM image of SiNWs etched for 7 min (**a**), high-magnification cross-section of the same image (**b**), and (**c**) top-view SEM image of SiNWs etched for 7 min.

From the SEM image analysis, the wire's cross-sectional surface coverage was estimated at roughly 28% by using the Gwyddion program, Figure 2. By counting the average number of wires on several line scans, the wire density was estimated to be 1.6×10^7 mm^2, which corresponds to roughly 8×10^8 wires under the force meter area (7 × 7 mm).

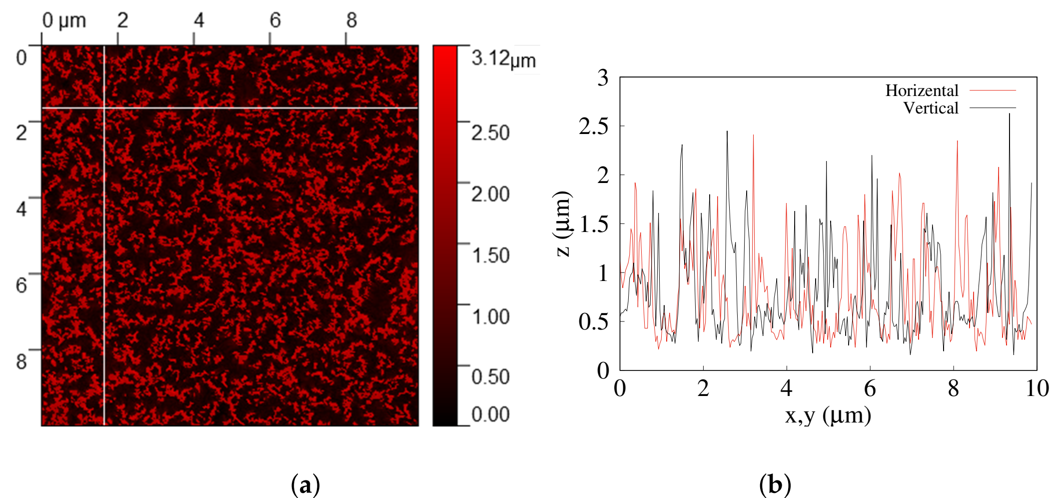

(**a**) (**b**)

Figure 2. (**a**) Gwyddion analysis of top-view SEM image in (100 µm^2). (**b**) Two Gwyddion line-scans of the figure to the left (red color—horizontal axis, black color—vertical axis).

2.2. Measurement Setups

For uniaxial PZR tests, the samples were clamped between a metal pin of a force meter (Mark-10, M5-012), touching the top side of the samples, and a rigid copper (Cu) plate at the backside, as shown in Figure 3. In order to improve the electrical contacts, the samples were glued to the Cu backside plate with silver paste. The force meter was mounted on a vertical rod allowing for movement on the *z*-axis (vertical) by a manually adjusted screw. Uniaxial pressure was applied to the samples by pressing the pin of the force meter into the samples' surface with an intensity determined by the aforementioned screw. The applied force was in the range of 100 mN to 900 mN on an area of 7 × 7 mm (the cross-sectional area of the pin). Taking the wire coverage (28 %) into account, this corresponds to a gauge pressure of 7 kPa to 66 kPa. Figure 3 shows a sketch of the experimental setup. A Keithley 2400 SourceMeter was used to measure the resistance *R* through the sample as a function of applied pressure at a constant bias voltage of 2 V.

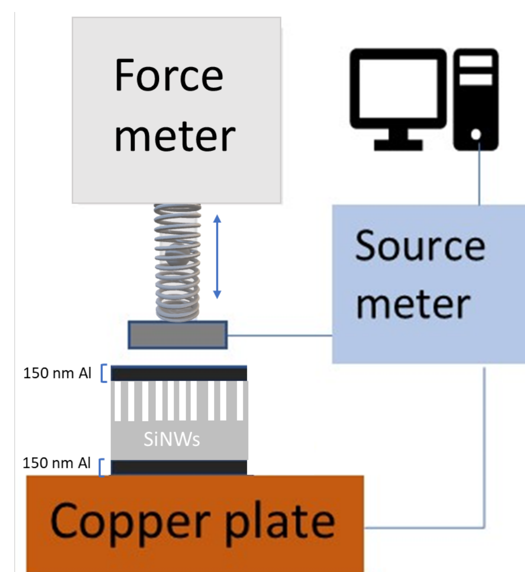

Figure 3. Schematic of the force meter setup for testing PZR characteristics.

For PZR tests under isostatic pressure variation, a vacuum chamber was used, and the air was removed while the resistance was measured at a fixed 5 V. In this case (for sample E), the contacts were made in co-planar configuration, with separate contacts on each side

of the patterned area, such that the nanowires are maximally exposed to air instead of top-and-bottom contacts as for the uniaxial measurements (performed with samples A–D). Furthermore, the wire length was increased (to 10 µm) to increase the surface area exposed to the air. The samples were mounted on a fixed sample station inside the chamber with tungsten needle tip kelvin probes as a connection.

3. Results

3.1. Electrical Response under Uniaxial Force

A maximum force of approximately 900 mN was applied to the samples using the setup shown in Figure 3. The maximum vertical force exerted on each wire thus corresponds to 900×10^{-3} N$/8 \times 10^{8} \approx 1.1 \times 10^{-9}$ N/wire or 6.6×10^{4} Pa (0.65 bar).

The force and the instantaneous resistance measured after applying the force to the sample with nanowires of length 3 µm (etched for 7 min) are shown in Figure 4a as a function of time. The maximum force was applied at the beginning (time zero) and then reduced step-wise while the resistance was being measured. Each force level was kept constant for roughly 50 s to confirm that the resistance value was stable with time. As clearly visible, the resistance changes significantly and inversely with pressure.

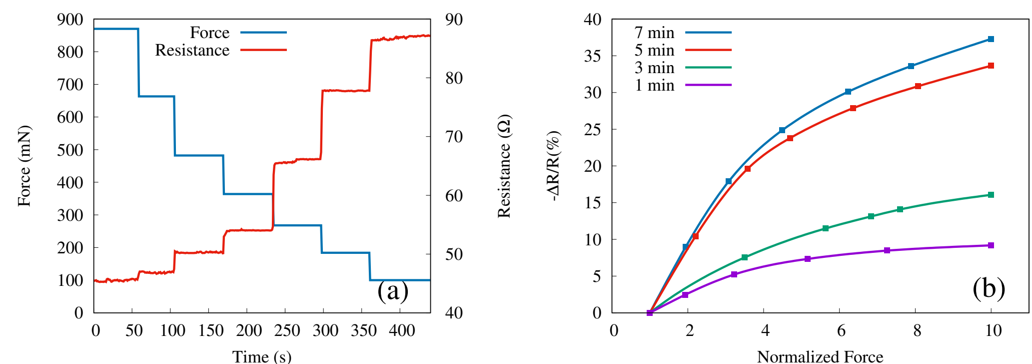

Figure 4. (**a**) Instantaneous resistance (right *y*-axis, red line) in response to applied force (left 4-axis, blue line) over time for sample D. (**b**) Relative resistance change versus normalized force for SiNWs samples A (purple), B (green), C (red), and D (blue).

We define the relative resistance change vs. force variation for each step $k = 1, 2, \ldots$ as

$$\frac{\Delta R}{R} = \frac{R_k - R_1}{R_1}, \tag{1}$$

where R_k is the average resistance obtained for the constant force step k. The measurements were repeated four times on each sample (A, B, C, D), each time reproducing the force steps as well as possible with the adjustable screw. A second average, this time of the relative resistance in step k, defined by Equation (1), obtained for the four measurements vs. the average normalized forces for each step, is presented in Figure 4b. Here, by normalized force, we mean the ratio of the force in a particular step k to the initial force, F_k/F_1. Hence, the maximum force values for each step-wise measurement are normalized to unity. Note that the resistance decreases when the force increases and that in Figure 4b, we show the negative of $\Delta R/R$.

Increasing the length of the nanowires (by increasing the etching time) leads to higher relative resistance, although the trend appears to saturate; only a relatively small difference between the 5 min and 7 min samples has been obtained. The highest relative change (37.3%) in resistance is observed for the longest etching time (sample D) with regards to uniaxial pressure.

In Figure 5, the resistance versus applied force is shown again for sample D (blue line), now compared with the case of the bulk Si (red line). For this measurement, we replicated sample D four times, in the same conditions of a 7 min etching time, and performed the

measurements on each sample replica. These measurements have been performed to test the repeatability of the sensor's response in the same conditions as have been performed in Figure 4a. It is worth noting that the un-uniform step size observed in Figure 4a is due to the manually adjustable screw of the force meter shown in the schematic. The data displayed are average values measured on these samples (D-like), shown with the error bars. A striking difference between these two configurations (SiNWs vs. bulk Si) is observed. No measurable change in resistance is seen for the bulk Si, in very sharp contrast to the SiNWs sample.

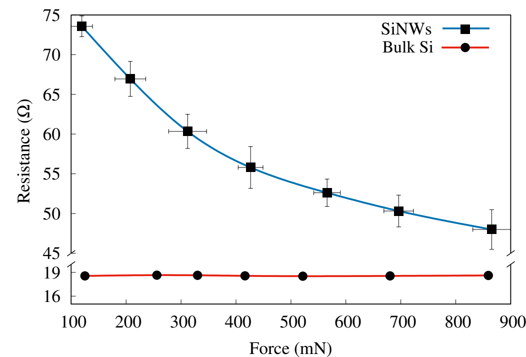

Figure 5. Resistance vs. applied force for the D-like samples (blue line) and bulk-Si (red line). Data for SiNWs are average values of four distinct samples; the error bars show the range in which the measurements fell.

Up to a 35 % change in resistivity was observed over the pressure variation in the range of 0.1 N to 0.9 N. In order to test the stability of SiNW's PZR response and response time, we performed several sets of measurements over different samples. In this stability test, the resistance shift was measured in periods of 60 s of loading and unloading force for all the samples. All samples were loaded by 860(10) mN and then unloaded to 220(10) mN. We observe a fast response (below 0.5 s), good stability, and high sensitivity to repeated pressure changes. The results of a reproducibility test for sample D are presented in Figure 6.

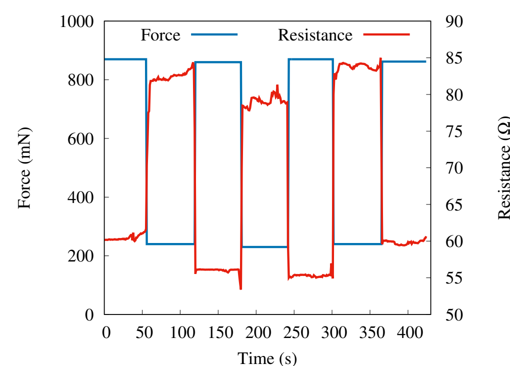

Figure 6. SiNWs PZR response due to repeated load–unload forces in real time for sample D.

Hydrogenation (exposure to hydrogen plasma) is widely used in the electronic industry to increase the mobility of charge carriers in semiconductors. It neutralizes deep and shallow defects and charged surface states [31,32]. Because the PZR effect has been attributed to surface states, we applied a hydrogenation treatment in order to explore the origin of the PZR effect in SiNWs. For hydrogen plasma treatment, we used a custom-built inductively coupled discharge setup with cylindrical geometry (290 mm long quartz tube with a diameter of 34 mm). The quartz tube was held inside a circular copper inductive coil with a diameter of 54 mm. A radio-frequency power generator CERSAR (c) (13.56 MHz) source coupled with an impedance-matching unit was utilized. For hydrogenation, a gas

mixture of Ar/H_2 (30 / −70%) was used, and the throttle valves were adjusted to stabilize the gas pressure of 29 mbar. A more detailed description and schematic of the hydrogenation setup can be found elsewhere [33,34]. In Figure 7, we compare the behavior of sample D before and after the hydrogenation. The PZR effect decreases dramatically and can be attributed to the passivation of the surface states [35].

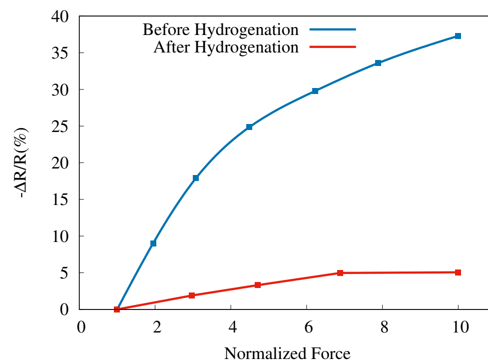

Figure 7. SiNWs PZR response for sample D before and after hydrogenation.

3.2. Electrical Response under Isostatic Pressure

Sample E (10 µm) was used for the investigation of the PZR response to isostatic pressure in a vacuum chamber. The PZR response was tested in the chamber under re-pressurizing conditions in the range of 10^{-4} mbar to 10^3 mbar. The results are shown in Figure 8, where the resistance is plotted as a function of the pressure measured at a fixed bias voltage of 5 V. We observed a dramatic increase in the resistance by more than two orders of magnitude when pumping the air out of the vacuum chamber. We believe this is a result of combined mechanical and chemical effects: the pressure drop removes mechanical stress, and the lack of air and humidity suppresses the chemisorption. Note that the resistance values for sample E are much higher than for samples A–D because of the co-planar configuration of the contacts and also because of the larger length of the nanowires.

In the Supplementary Material we show, for comparison, the behavior of periodic arrays of SiNWs with increasing isostatic pressure.

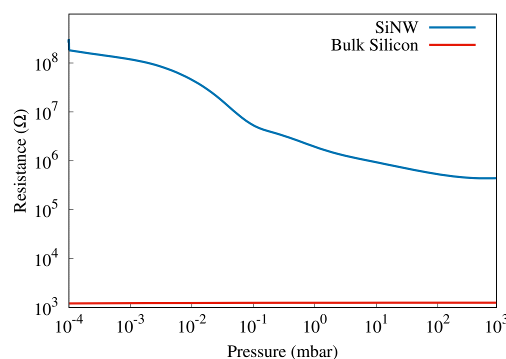

Figure 8. The resistance of sample E (on a log 10 scale) as a function of pressure measured in the vacuum chamber is shown with the blue curve. For comparison, in red, the resistance of a bulk silicon sample (i.e., without nanowires).

4. Discussion

For solid materials, the inter-atomic spacing may be altered by strain. Consequently, apart from geometric changes in semiconductors, bandstructure-related details, such as bandgap or effective mass, may change, and thereby the resistivity may change as well. An applied strain changes the bandgap and the effective mass of charge carriers, which, in

turn, affect the carrier concentration as well as their mobility [36]. Within a certain range of strain, this relationship is linear [22,37]. Niquet et al. [36] show that electron mobility saturates with strain. Subsequently, the PZR response saturates above a certain range of strain. When a uniaxial stress X is applied, the piezoresistance coefficient of the resistivity ρ in the direction of stress is defined as

$$\pi_l = \frac{\Delta\rho}{\rho_0}\frac{1}{X}\,, \tag{2}$$

where $\Delta\rho$ is the stress-induced change in the resistivity and ρ_0 is the reference resistivity of the unstressed material.

In our case, a uniaxial compressive force F was applied to SiNWs along their length by a force meter. The stress is $X = F/A_{\mathrm{t}}$, A_{t} being the total cross-sectional area of the nanowires, which is equal to pA_{m}, where A_{m} is the cross-sectional area of the pin pressed into the wires, and p is the relative cross-sectional area of the wires. Assuming the electrical resistivity of the nanowires is proportional to their resistance, Equation (2) becomes

$$\pi_l = \frac{pA_{\mathrm{m}}}{F} \times \frac{\Delta R}{R_0}\,. \tag{3}$$

The structure of our SiNWs array is robust and stable as the wires are partially interconnected, which provides high structural strength. Such stability and fast response of SiNWs is a desired property for many devices, such as solid-state accelerometers and bipolar transistors [38]. Further, our results are in agreement with the study of Ghosh et al. [19], in which large-diameter Si nanorod-based sensors were used for force detection.

He et al. [13], who measured PZR coefficients of single (p-doped) SiNWs, with diameters 50 nm to 300 nm, made from wafers with resistivities of 0.003 Ω cm to 10 Ω cm, found that the PZR was roughly inversely proportional to the diameter and proportional to the wafer resistivity. For a similar diameter and wafer resistivity as in our present work, ∼150 nm and 10 Ω cm, respectively, the PZR coefficient π_l for a single wire was of the order $10^{-7}\,\mathrm{Pa}^{-1}$. (According to Figure 2d of Ref. [13]). Using Equation (3), with $p = 0.28$, $A_m = 49\,\mathrm{mm}^2$, $F = 0.8\,\mathrm{N}$, and $\Delta R/R = 0.35$, we obtain $\pi_l \approx 6 \times 10^{-6}\,\mathrm{Pa}^{-1}$, i.e., almost two orders of magnitude higher. Note that, in principle, Equation (2) does not depend on sample details, such as the number of nanowires or their configuration, which we believe plays a role in our case. Therefore, we attribute this higher value to a collective PZR effect brought about by the interaction between multiple and interconnected wires rather than the response of a single nanowire. Additionally, the pressure sensitivity of the sensor in the isostatic pressure variation given by $S = \frac{\Delta R}{R}/\Delta P$ [39], in the pressure range of 10^{-4} to 10^3 mbar, is $9.98 \times 10^{-6}\,\mathrm{Pa}^{-1}$. It is also seen that the highest sensitivity (highest slope in Figure 8) is found in the pressure range of roughly 10^{-2} and 10^{-1} mbar where the sensitivity measure is $8.8 \times 10^{-3}\,\mathrm{Pa}^{-1}$.

5. Conclusions

In summary, large arrays of interconnected SiNWs were fabricated in a simple three-step wet chemical process and used for testing the piezoresistance effect in nanowires. The interconnected structures of the SiNWs provide a great increase in mechanical stability. A pressure change of 100 Pa could be measured with this robust device. The calculated PZR coefficient based on SiNWs array with NWs length of 3 µm as resulted after MACE etching for 7 min, sample D, was almost two orders of magnitude higher for our sensor than reported for a single SiNW. Repeated measurements for different samples fabricated with the same process demonstrated good reproducibility with less than 5% deviation in pressure sensing. The electrical resistance of SiNWs of 10 µm length increased more than two orders of magnitude when measured in a vacuum. These findings make the device based on random and interconnected SiNWs a strong candidate as a simple and inexpensive alternative to various pressure-sensing applications.

Supplementary Materials: The following supporting information can be downloaded at: https://www.mdpi.com/article/10.3390/s22176340/s1, Figure S1: Cross-sectional SEM micrographs of periodic SiNWs-ZnO array with wire length of 650 nm, inset shows the top view image; Figure S2: (a) I-V characteristics for direct bias of the 650 nm periodic SiNWs, with applied pressure in the range 0.5–3.5 MPa. The blue curve corresponds to atmospheric pressure. (b) Variation of $\Delta R/R_0$ with applied pressure for a fixed direct bias of 2 V.

Author Contributions: Conceptualization, R.P.; Funding acquisition, H.G.S.; Investigation, E.F., M.T.S., T.H.K. and H.Ö.Á.; Methodology, E.F., M.T.S. and H.G.S.; Project administration, R.P., N.P., A.M. and H.G.S.; Supervision, R.P., N.P., A.M., S.I. and H.G.S.; Visualization, H.G.S.; Writing—original draft, E.F.; Writing—review & editing, M.T.S., A.M., S.I. and H.G.S. All authors have read and agreed to the published version of the manuscript.

Funding: This work was supported by Reykjavik University Ph.D. fund No. 220006, and funding from the Icelandic Research Fund Grant No. 218029-051. RP acknowledges support from the Romanian Core Program Contract No.14 N/2019 Ministry of Research, Innovation, and Digitalization.

Institutional Review Board Statement: Not applicable.

Informed Consent Statement: Not applicable.

Data Availability Statement: Not applicable.

Conflicts of Interest: The authors declare no conflict of interest.

References

1. Peng, K.Q.; Wang, X.; Li, L.; Hu, Y.; Lee, S.T. Silicon nanowires for advanced energy conversion and storage. *Nano Today* **2013**, *8*, 75–97. [CrossRef]
2. Heris, H.R.; Kateb, M.; Erlingsson, S.I.; Manolescu, A. Thermoelectric properties of tubular nanowires in the presence of a transverse magnetic field. *Nanotechnology* **2020**, *31*, 424006. [CrossRef] [PubMed]
3. Heris, H.R.; Kateb, M.; Erlingsson, S.I.; Manolescu, A. Effects of transverse geometry on the thermal conductivity of Si and Ge nanowires. *Surf. Interfaces* **2022**, *30*, 101834. [CrossRef]
4. Zhou, X.; Hu, J.; Li, C.; Ma, D.; Lee, C.; Lee, S. Silicon nanowires as chemical sensors. *Chem. Phys. Lett.* **2003**, *369*, 220–224. [CrossRef]
5. Peng, K.Q.; Wang, X.; Lee, S.T. Gas sensing properties of single crystalline porous silicon nanowires. *Appl. Phys. Lett.* **2009**, *95*, 243112. [CrossRef]
6. Smith, C.S. Piezoresistance effect in germanium and silicon. *Phys. Rev.* **1954**, *94*, 42–49. [CrossRef]
7. Tufte, O.N.; Chapman, P.D.; Long, D. Silicon diffused-element piezoresistive diaphragms. *J. Appl. Phys.* **1962**, *33*, 3322–3327. [CrossRef]
8. Tortonese, M.; Barrett, R.C.; Quate, C.F. Atomic resolution with an atomic force microscope using piezoresistive detection. *Appl. Phys. Lett.* **1993**, *62*, 834. [CrossRef]
9. Ning, Y.; Loke, Y.; McKinnon, G. Fabrication and characterization of high g-force, silicon piezoresistive accelerometers. *Sens. Actuators A Phys.* **1995**, *48*, 55–61. [CrossRef]
10. Wee, K.; Kang, G.; Park, J.; Kang, J.; Yoon, D.; Park, J.; Kim, T. Novel electrical detection of label-free disease marker proteins using piezoresistive self-sensing micro-cantilevers. *Biosens. Bioelectron.* **2005**, *20*, 1932–1938. [CrossRef]
11. Tiwari, B.; Billot, M.; Clévy, C.; Agnus, J.; Piat, E.; Lutz, P. A two-axis piezoresistive force sensing tool for microgripping. *Sensors* **2021**, *21*, 6059. [CrossRef] [PubMed]
12. Dorda, G. Piezoresistance in quantized conduction bands in silicon inversion layers. *J. Appl. Phys.* **1971**, *42*, 2053–2060. [CrossRef]
13. He, R.; Yang, P. Giant piezoresistance effect in silicon nanowires. *Nat. Nanotechnol.* **2006**, *1*, 42–46. [CrossRef] [PubMed]
14. Gao, D.; Yang, Z.; Zheng, L.; Kun, Z. Piezoresistive effect of n-type <111> -oriented Si nanowires under large tension/compression. *Nanotechnology* **2017**, *28*, 095702. [PubMed]
15. Zhang, S.; Lou, L.; Lee, C. Piezoresistive silicon nanowire based nanoelectromechanical system cantilever air flow sensor. *Appl. Phys. Lett.* **2012**, *100*, 023111. [CrossRef]
16. Cheng, W.; Yu, L.; Kong, D.; Yu, Z.; Wang, H.; Ma, Z.; Wang, Y.; Wang, J.; Pan, L.; Shi, Y. Fast-response and low-hysteresis flexible pressure sensor based on silicon nanowires. *IEEE Electron Device Lett.* **2018**, *39*, 1069–1072. [CrossRef]
17. Nguyen, T.D.; Lee, J.S. Recent Development of Flexible Tactile Sensors and Their Applications. *Sensors* **2021**, *22*, 50. [CrossRef]
18. Kim, C.; Ahn, H.; Ji, T. Flexible Pressure Sensors Based on Silicon Nanowire Array Built by Metal-Assisted Chemical Etching. *IEEE Electron Device Lett.* **2020**, *41*, 1233–1236. [CrossRef]
19. Ghosh, R.; Song, M.S.; Park, J.; Tchoe, Y.; Guha, P.; Lee, W.; Lim, Y.; Kim, B.; Kim, S.W.; Kim, M.; et al. Fabrication of piezoresistive Si nanorod-based pressure sensor arrays: A promising candidate for portable breath monitoring devices. *Nano Energy* **2021**, *80*, 105537. [CrossRef]

20. Shiri, D.; Kong, Y.; Buin, A.; Anantram, M.P. Strain induced change of bandgap and effective mass in silicon nanowires. *Appl. Phys. Lett.* **2008**, *93*, 07314. [CrossRef]
21. Zhang, J.; Zhao, Y.; Ge, Y.; Li, M.; Yang, L.; Mao, X. Design optimization and fabrication of high-sensitivity SOI pressure sensors with high signal-to-noise ratios based on silicon nanowire piezoresistors. *Micromachines* **2016**, *7*, 187. [CrossRef] [PubMed]
22. Rowe, A. Piezoresistance in silicon and its nanostructures. *J. Mater. Res.* **2014**, *29*, 731–744. [CrossRef]
23. Toriyama, T.; Tanimoto, Y.; Sugiyama, S. Single crystal silicon nano-wire piezoresistors for mechanical sensors. *J. Microelectromechanical Syst.* **2002**, *11*, 605–611. [CrossRef]
24. Toriyama, T.; Sugiyama, S. Single crystal silicon piezoresistive nano-wire bridge. *Sens. Actuators A Phys.* **2003**, *108*, 244–249. [CrossRef]
25. Schmidt, V.; Wittemann, J.V.; Senz, S.; Gösele, U. Silicon nanowires: A review on aspects of their growth and their electrical properties. *Adv. Mater.* **2009**, *21*, 2681–2702. [CrossRef]
26. Shi, D.; Chen, Y.; Li, Z.; Dong, S.; Li, L.; Hou, M.; Liu, H.; Zhao, S.; Chen, X.; Wong, C.P.; et al. Anisotropic Charge Transport Enabling High-Throughput and High-Aspect-Ratio Wet Etching of Silicon Carbide. *Small Methods* **2022**, 6, 2200329. [CrossRef]
27. Svavarsson H.G.; Hallgrimsson, B.H.; Niraula, M.; Lee K.J.; Magnusson, R. Large arrays of ultra-high aspect ratio periodic silicon nanowires obtained via top-down route. *Appl. Phys. A-Mater. Sci. Process.* **2016**, *122*, 1–6. [CrossRef]
28. Fakhri, E.; Sultan, M.; Manolescu, A.; Ingvarsson, S.; Plugaru, N.; Plugaru, R.; Svavarsson, H. Synthesis and photoluminescence study of silicon nanowires obtained by metal assisted chemical etching. In Proceedings of the 2021 International Semiconductor Conference (CAS), Sinaia, Romania, 6–8 October 2021; pp. 147–150.
29. Plugaru, R.; Fakhri, E.; Romanitan, C.; Mihalache, I.; Craciun, G.; Plugaru, N.; Árnason, H.O.; Sultan, M.T.; Nemnes, G.A.; Ingvarsson, S.; et al. Structure and electrical behavior of silicon nanowires prepared by MACE process. *arXiv* **2022**, arXiv:2206.05006
30. Neuzil, P.; Wong, C.C.; Reboud, J. Electrically controlled giant piezoresistance in silicon nanowires. *Nano Lett.* **2010**, *10*, 1248–1252. [CrossRef]
31. Danielsson, D.; Gudmundsson, J.; Svavarsson, H. Effect of hydrogenation on minority carrier lifetime in low-grade silicon. *Phys. Scr.* **2010**, *2010*, 014005. [CrossRef]
32. Svavarsson, H.G.; Sultan, M.T.; Lee, K.J.; Magnusson, R. Hydrogenated silicon films for low-loss resonant reflectors operating in the visible region. In Proceedings of the 2020 IEEE Research and Applications of Photonics, Miramar Beach, FL, USA, 10–12 August 2020; pp. 1–2.
33. Sultan, M.; Gudmundsson, J.T.; Manolescu, A.; Stoica, T.; Ciurea, M.; Svavarsson, H. Enhanced photoconductivity of embedded SiGe nanoparticles by hydrogenation. *Appl. Surf. Sci.* **2019**, *479*, 403–409. [CrossRef]
34. Sultan, M.; Gudmundsson, J.T.; Manolescu, A.; Ciurea, M.; Svavarsson, H. The Effect of H 2/Ar Plasma Treatment Over Photoconductivity of Sige Nanoparticles Sandwiched Between Silicon Oxide Matrix. In Proceedings of the 2018 International Semiconductor Conference (CAS), Sinaia, Romania, 10–12 October 2018; pp. 257–260.
35. Song, L.; Yang, D.; Yu, X. Investigation on the impact of hydrogen on the passivation of silicon surface states in clean and copper contaminated conditions. *AIP Adv.* **2019**, *9*, 105102. [CrossRef]
36. Niquet, Y.M.; Delerue, C.; Krzeminski, C. Effects of strain on the carrier mobility in silicon nanowires. *Nano Lett.* **2012**, *12*, 3545–3550. [CrossRef]
37. Matsuda, K.; Suzuki, K.; Yamamura, K.; Kanda, Y. Nonlinear piezoresistance effects in silicon. *J. Appl. Phys.* **1993**, *73*, 1838–1847. [CrossRef]
38. Doll, J.C.; Pruitt, B.L. *Piezoresistor Design and Applications*; Springer: Berlin, Germany, 2013.
39. Pataniya, P.M.; Bhakhar, S.A.; Tannarana, M.; Zankat, C.; Patel, V.; Solanki, G.; Patel, K.; Jha, P.K.; Late, D.J.; Sumesh, C. Highly sensitive and flexible pressure sensor based on two-dimensional MoSe2 nanosheets for online wrist pulse monitoring. *J. Colloid Interface Sci.* **2021**, *584*, 495–504. [CrossRef] [PubMed]